Coding of Temporally Varying Signals in Networks of Spiking Neurons with Global Delayed Feedback

Naoki Masuda
masuda@brain.riken.jp
Laboratory for Mathematical Neuroscience, RIKEN Brain Science Institute, Wako, Japan, and ERATO Aihara Complexity Modelling Project, Japan Science and Technology Agency, Tokyo, Japan

Brent Doiron
bdoiron@science.uottawa.ca
Physics Department, University of Ottawa, Ottawa, Canada, and Department of Cellular and Molecular Medicine, University of Ottawa, Ottawa, Canada

André Longtin
alongtin@physics.uottawa.ca
Physics Department, University of Ottawa, Ottawa, Canada

Kazuyuki Aihara
aihara@sat.t.u-tokyo.ac.jp
Department of Complexity Science and Engineering, Graduate School of Frontier Sciences, University of Tokyo, Tokyo, Japan, and ERATO Aihara Complexity Modelling Project, Japan Science and Technology Agency, Tokyo, Japan

Oscillatory and synchronized neural activities are commonly found in the brain, and evidence suggests that many of them are caused by global feedback. Their mechanisms and roles in information processing have been discussed often using purely feedforward networks or recurrent networks with constant inputs. On the other hand, real recurrent neural networks are abundant and continually receive information-rich inputs from the outside environment or other parts of the brain. We examine how feedforward networks of spiking neurons with delayed global feedback process information about temporally changing inputs. We show that the network behavior is more synchronous as well as more correlated with and phase-locked to the stimulus when the stimulus frequency is resonant with the inherent frequency of the neuron or that of the network oscillation generated by the feedback architecture. The two eigenmodes have distinct dynamical characteristics, which are supported by numerical simulations and by analytical arguments based on frequency response and bifurcation theory. This distinction is similar to the class I versus class II classification of single neurons according to the bifurcation from

quiescence to periodic firing, and the two modes depend differently on system parameters. These two mechanisms may be associated with different types of information processing.

1 Introduction

1.1 Oscillations and Synchrony in Feedforward Networks. Oscillatory and synchronous activities of field potentials and neuronal firing are widely found in various parts of the brain. Accordingly, their functional roles beyond the classical notion of rate coding have been widely debated. For example, oscillatory synchrony in the γ band around 40 Hz of distant neurons with nonoverlapping receptive fields may bind features of the presented stimuli, as supported by the recordings in the visual cortex (Gray, König, Engel, & Singer, 1989; Llinás, Grace, & Yarom, 1991; Sillito, Jones, Gerstein, & West, 1994; Douglas, Koch, Mahowald, Martin, & Suarez, 1995; Ritz & Sejnowski, 1997; Murphy, Duckett, & Sillito, 1999) and the olfactory system (Stopfer, Bhagavan, Smith, & Laurent, 1997). Such oscillations are also used by the electric fish for communication between conspecific (Heiligenberg, 1991). On the other hand, θ oscillations (8–12 Hz) in the hippocampus are suspected of giving information on contexts or on behavioral states to upstream neurons, supplying them with precise temporal structure (Klausberger et al., 2003; Buzsáki & Draguhn, 2004). Model studies with feedforward networks also support the role for oscillatory synchrony in promoting phase locking of spikes onto external stimuli (Hopfield, 1995; Gerstner, Kempter, van Hemmen, & Wagner, 1996). Precisely timed spiking is necessary, for example, in auditory sensation, which requires coincidence detection with high temporal resolution and enhanced reliability of spiking (Gerstner et al., 1996; Hunter, Milton, Thomas, & Cowan, 1998).

The meaning of synchronous firing (oscillatory and nonoscillatory) has been widely discussed, for example, with the synfire chain models in which the volleys of synchronous firing are propagated in networks to transmit and process the inputs (Abeles, 1991). How neural networks encode stimulus information in relation to synchrony and/or asynchrony has particularly been examined with feedforward networks, which are more amenable to analyses. In feedforward networks, synchronous and asynchronous states alternate when the network parameters are modulated (Gerstner & Kistler, 2002; Masuda & Aihara, 2002b, 2003a; van Rossum, Turrigiano, & Nelson, 2002; Nirenberg & Latham, 2003). For a small amount of noise or relatively homogeneous networks, the likely behavior is synchronous firing, which may be related to binding or the synfire chain (Abeles, 1991; Diesmann, Gewaltig, & Aertsen, 1999; Câteau & Fukai, 2001; van Rossum et al., 2002; Aviel, Mehring, Abeles, & Horn, 2003; Litvak, Sompolinsky, Segev, & Abeles, 2003; Mehring, Hehl, Kubo, Diesmann, & Aertsen, 2003; Reyes, 2003).

Conversely, large noise or heterogeneity tends to result in asynchronous firing that is advantageous for the population firing rate coding of stimuli with high temporal resolution (Shadlen & Newsome, 1998; Masuda & Aihara, 2002b; van Rossum et al., 2002) and for rapidly responding to stimulus changes (Gerstner, 2000; Gerstner & Kistler, 2002).

1.2 Feedback Links Oscillations and Synchrony. Although the model analyses mentioned so far and many others use feedforward architecture, purely feedforward circuits are rarely found in biological neural networks. Little is known about how recurrent networks behave in terms of synchrony and coding in the context of time-dependent inputs. This is the question that our article addresses. Nervous systems are full of feedback loops ranging from the level of a small number of neurons (Berman & Maler, 1999; Wilson, 1999) to the level of the brain areas (Damasio, 1989; Llinás et al., 1991; Ritz & Sejnowski, 1997). Remarkably, in the visual cortex, the inputs relayed from the global feedback pathway outnumber by far the feedforward ones such as sensory inputs (Douglas et al., 1995; Billock, 1997).

Accordingly, information processing that is unexpected of feedforward networks could exist in networks in which the feedforward and feedback signals are mixed. An apparent role for the global feedback is to enhance synchrony of the upstream neurons, which are more related to peripheral nervous system than are the downstream neurons located closer to the central nervous system. This enhanced synchrony is found in the thalamocortical pathway (Sillito et al., 1994; Bal, Debay, & Destexhe, 2000), the basal ganglia (Plenz & Kitai, 1999), and the olfactory system (Stopfer et al., 1997). In recurrent networks, synchrony is enhanced because the feedback signals serve as common inputs to the upstream neurons, which generally make the neurons more synchronous (Knight, 1972; Shadlen & Newsome, 1998; Gerstner, 2000; Masuda & Aihara, 2002b, 2003b; Aviel et al., 2003; Mehring et al., 2003). Synchrony probably encodes the stimulus information, for example, on the orientation of visual stimuli (Sillito et al., 1994; Douglas et al., 1995; Murphy et al., 1999). Synchrony accompanied by the fine temporal structure of spike trains, which is induced by the correlated feedback, may also be useful in more general spatiotemporal spike codings. Examples include synfire chains embedded in recurrent neural networks (Aviel et al., 2003; Mehring et al., 2003), binding of the fragmental stimulus information that reverberates in the feedback loops (Damasio, 1989; Billock, 1997; Buzsáki & Draguhn, 2004), temporal filling in of visual stimuli (Billock, 1997), selective attention (Billock, 1997), and signal restoration (Douglas et al., 1995). Another important role for global feedback is to induce oscillations with period specified by the loopback time (Wilson, 1999; Doiron, Chacron, Maler, Longtin, & Bastian, 2003). In summary, oscillations and synchronization are in close relation with each other when both are mediated by global delayed feedback.

1.3 Recurrent Nets with Dynamic Inputs. The mechanisms of synchronization and oscillations in recurrent networks have been extensively studied with models. However, most of them assume constant or simple noisy external inputs whose information content is limited to a few static quantities such as the levels of biases and noise (Abeles, 1991; Diesmann et al., 1999; Brunel & Hakim, 1999; Brunel, 2000; Doiron et al., 2003; Doiron, Lindner, Longtin, Maler, & Bastian, 2004). Accordingly, how oscillatory synchrony interacts with external inputs and how the input information is processed have not been discussed, with few exceptions (Knight, 2000; Gerstner & Kistler, 2002). Actually, external inputs often have their own timescales and spatiotemporal structure (Gerstner et al., 1996), and they may interact with the dynamic properties of neural networks to affect the way in which information is processed (Doiron et al., 2003; Chacron, Doiron, Maler, Longtin, & Bastian, 2003).

In addition, most studies on synchrony and oscillations in neural networks have ignored the effects of single neurons, which have their own timescales of firing according to bias strength and noise level (Knight, 1972; Aihara & Matsumoto, 1982; Llinás et al., 1991; Longtin, 1995, 2000; Izhikevich, Desai, Walcott, & Hoppensteadt, 2003; Buzsáki & Draguhn, 2004). When the eigenfrequency of a single neuron is resonant with the input frequency, signal amplification and better performance of the coding happen in both the subthreshold and suprathreshold regimes (Knight, 1972, 2000; Hunter et al., 1998; Longtin & St-Hilaire, 2000; Longtin, 2000; Gerstner & Kistler, 2002; Lindner & Schimansky-Geier, 2002; Masuda & Aihara, 2003c). Then it is possible that three timescales, each originating from the global feedback, the single-neuron property, or the inputs, coexist and interact in one neural system. The distinction between resonant and nonresonant behaviors is particularly important in this respect.

1.4 Outline of Our Letter. Our focus in this letter is on analyzing information processing of temporally changing inputs by noisy spiking neural networks with global feedback. To this end, we use inputs with temporal structure, mostly sinusoidal inputs. The reason for this choice is twofold. One is that sinusoidal waves are established as standard tools for dynamical systems, as represented by transfer functions and resonance analysis. The second is that animals often receive natural sinusoidal-like inputs. For example, pure tone auditory inputs are sinusoidal waves, and they are processed frequency-wise in auditory pathways (Gerstner et al., 1996). Electrosensory systems of weakly electric fish also receive periodic inputs for communication (Heiligenberg, 1991). Regular respiratory rhythm also affects dynamics and functions of olfactory systems (Fontanini, Spano, & Bower, 2003). We ignore spatial features of signals and networks, which is another interesting topic (van Rossum et al., 2002; Doiron et al., 2003, 2004); thus our networks have homogeneous coupling structure.

In section 2, we introduce the network model with two layers of neurons with spiking dynamics. In section 3, we examine how synchrony, oscillations, and asynchrony are determined by the strength of the global feedback. Section 4 is devoted to the numerical analysis of how the frequency information in inputs is processed by the network in relation to resonances between different time constants. We analyze the resonance phenomena with the use of the dynamical model for population activity (Gerstner, 2000; Gerstner & Kistler, 2002) in section 5. Accordingly, two complementary calculations are presented: linear analysis based on gain functions in the frequency domain in section 6 and nonlinear analysis based on the bifurcation theory in section 7. In section 8, we discuss differences in the functional consequences of the single-neuron dynamics and those of the global feedback loops, with possible relevance to experiments.

2 Model

2.1 Dynamical Equations. The feedforward neural network with global feedback that we use in this letter is schematically shown in Figure 1. The network contains two layers, A and B, of noisy leaky integrate-and-fire (LIF) neurons (Knight, 1972; Gerstner & Kistler, 2002) with the membrane time constant $\tau_m = 20.0$ ms. It is supposed to model two mutually connected regions of the brain, such as two different layers in a columnar structure, a thalamocortical loop, or interacting excitatory and inhibitory thalamic nuclei. Layer A consists of $n_1 = 250$ neurons that receive common external inputs. The downstream layer B has $n_2 = 30$ neurons, each of which receives feedforward spike inputs from $n_1' = 75$ randomly chosen neurons in layer A. Every neuron in layer B transmits spike trains back to all the neurons in layer A, modeling a global feedback loop. It provides correlated inputs

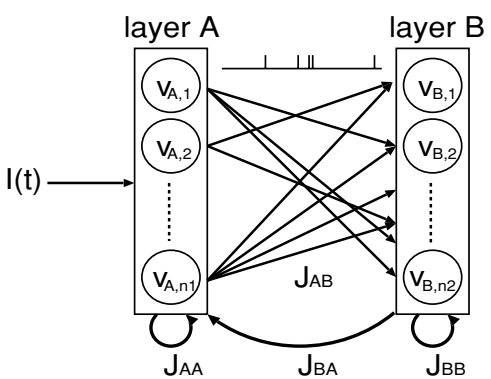

Figure 1: Architecture of the feedforward neural network with global feedback.

that tend to induce synchrony, which will be investigated in section 3. Each layer is also supplied with some intralayer excitatory coupling. However, we focus on global feedback instead of analyzing effects of intralayer feedback. Accordingly, the corresponding coupling constants (J_{AA} in equation 2.1 and J_{BB} in equation 2.2) are set rather arbitrarily at small values.

We use spatially homogeneous time-dependent external inputs $I(t)$. Although we exclusively use suprathreshold inputs, qualitatively similar results are expected for noisy subthreshold inputs based on single-cell modeling studies (Longtin & St-Hilaire, 2000; Longtin, 2000).

Let us denote the membrane potential of the ith neuron in layer A (resp. B) by $v_{A,i}$ (resp. $v_{B,i}$) and assume that each neuron has a threshold equal to 1. Upon firing, the membrane potentials are instantaneously reset to the resting potential 0, and the neurons restart integrating inputs. Then the dynamics of the whole network follows the stochastic delay differential equations written by

$$\begin{aligned}\tau_m \frac{dv_{A,i}}{dt} = &\sum_{i'=1}^{n_1} \sum_j J_{AA}\, \delta(t - T_{A,i',j} - \tau_{AA}) \\ &+ \sum_{i'=1}^{n_2} \sum_j J_{BA}\, \delta(t - T_{B,i',j} - \tau_{BA}) \\ &- v_{A,i}(t) + I(t) + \hat{\sigma}\xi_{A,i}(t),\ (1 \le i \le n_1) \qquad (2.1)\end{aligned}$$

$$\begin{aligned}\tau_m \frac{dv_{B,i}}{dt} = &\sum_{i' \in S_i} \sum_j J_{AB}\, \delta(t - T_{A,i',j} - \tau_{AB}) \\ &+ \sum_{i'=1}^{n_2} \sum_j J_{BB}\, \delta(t - T_{B,i',j} - \tau_{BB}) \\ &- v_{B,i}(t) + \hat{\sigma}\xi_{B,i}(t), (1 \le i \le n_2), \qquad (2.2)\end{aligned}$$

where δ is the delta function that approximates the interaction via action potentials, $t = T_{A,i',j}$ (resp. $T_{B,i',j}$) is the jth firing time of the i'th neuron in layer A (resp. B), and S_i is the set of neurons in layer A that project synapses onto the ith neuron in layer B. The coupling within each layer has the spike amplitude $J_{AA} = J_{BB} = 0.005$ and the propagation delay $\tau_{AA} = \tau_{BB} = 2.0$ ms. The feedforward coupling is assumed to have strength $J_{AB} = 0.5$ and to be instantaneous ($\tau_{AB} = 0$). The global feedback has a delay τ_{BA} and strength J_{BA}. Finally, the terms with ξ represent dynamical white gaussian noise with amplitude $\hat{\sigma}$ and are independent for all the neurons. We use the Euler-Maruyama integration scheme to numerically explore the system (Risken, 1984). We add independent white gaussian variables with variance σ^2 to the membrane potentials every $\Delta t = 0.02$ ms ($\hat{\sigma} = \sigma\sqrt{\Delta t}$). The results

in the following sections do not depend qualitatively on the parameter values.

2.2 Rationale for Model Formulation. Let us comment on the rationality and the limits of the assumptions. The instantaneous feedforward coupling is not realistic. However, this assumption is not essential because only lengths of feedback loops, namely, $\tau_{AB} + \tau_{BA}$, τ_{AA}, and τ_{BB}, matter for the resonance phenomena that turn out to be functionally important. This point is verified in section 6 with equations 6.8 and B.3.

Regarding the individuality of synapses, synaptic time delays from a specific subpopulation to another should be homogeneous enough for input coding supported by synchrony. This requirement is common to a body of work on the possibility of stable emergence of synchrony even with realistic conductance-based LIF neurons (Diesmann et al., 1999; Brunel, 2000; Doiron et al., 2003; Mehring et al., 2003). Therefore, we confine ourselves to the case in which the propagation delay is entirely homogeneous.

Another remark is that we set the intralayer propagation delays, or τ_{AA} and τ_{BB}, small compared to interlayer ones, or τ_{BA}, which are of the order of 10 ms in later sections. Biologically, delays in corticocortical horizontal connections are often long (Gilbert & Wiesel, 1983; Bringuier, Chavane, Glaeser, & Frégnac, 1999). Our focus is not on this type of networks, but on explaining other systems where effects of organized global feedback with relatively long delays are prominent. Examples include thalamic excitatory-inhibitory loops and thalamocortical loops (Destexhe & Sejnowski, 2003) and electrosensory systems (Heiligenberg, 1991). We could apply our results to, for example, corticocortical networks with slow intralayer interaction since values of τ_{AA} or τ_{BB} turn out to set oscillation frequencies of our interest, as will be later suggested by equation 6.8. However, this analogy is valid only when delays are more or less homogeneous and connections are statistically random, as mentioned above. These conditions are often violated particularly in view that horizontal coupling is not random but spatially organized (Gilbert & Wiesel, 1983; Bringuier et al., 1999; Mehring et al., 2003).

Last, with regard to the characteristics of noise, our independent white gaussian noise sources set the part of spontaneous activity independent for all the neurons, such as fluctuations at individual synapses due to stochastic synaptic releases. In reality, some parts of the fluctuations are spatially correlated because of shared synaptic inputs (Abeles, 1991; Shadlen & Newsome, 1998). To take into account the degree of input correlation is well beyond the scope of this work. However, based on the related results (Doiron et al., 2004), we anticipate that input correlation enhances the degree of synchrony, which is a key to efficiently encoding sinusoidal inputs.

2.3 Measures of Synchrony and Correlation. We introduce measures to evaluate the following coding properties: (1) the performance of the population rate coding, (2) the degree of synchrony, and (3) the frequency profile

of population firing rates. The last one is closely related to phase locking and temporal spike coding (Longtin, 1995; Gerstner et al., 1996) and also useful in evaluating the bandpass property in section 4. We measure property (1) by *corr*, which is defined to be the cross-correlation function between the temporally discretized versions of the inputs $\{s_1(i)\}$ and the population firing rates $\{s_2(i)\}$ (Masuda & Aihara, 2002b, 2003a). These time series are defined by

$$s_1(i) = \frac{1}{w}\int_{(i-1)w}^{iw} I(t)dt, \tag{2.3}$$

and

$$s_2(i) = \text{ the number of spikes from layer } A \text{ observed for } t \in [(i-1)w, iw), \tag{2.4}$$

where w is the width of the observation bin. We remark that in the limit of $w \to 0$, n_1 should tend to ∞, and with the proper normalization, $s_2(i)$ is the instantaneous firing probability of a neuron in layer A. The measure for property (2) is given by Burkitt and Clark (2001) and Masuda and Aihara (2002b):

$$r = \left|\sum_{j=1}^{n_1} \mathrm{e}^{2\pi i v_{A,j}(t)}\right| \Big/ n_1. \tag{2.5}$$

Stronger synchrony gives a larger value of r, and r is normalized in $[0, 1]$. Finally, the standard power spectrum of $\{s_2(i)\}$ is used to evaluate property (3). These measures are averaged over five trials, and each is calculated from the spike trains for the duration of 40 spikes from a single neuron.

3 Effects of Global Feedback on Synchrony

As a preliminary step for understanding how the network deals with temporally structured inputs, we first apply correlated noisy inputs and explore the effects of global feedback on population rate coding and synchrony. We use inputs generated by the Ornstein-Uhlenbeck process $\eta(t)$ whose dynamics are represented by

$$I(t) = I_0 + C\eta(t), \tag{3.1}$$

$$\tau_{OU}\frac{d\eta(t)}{dt} = -\eta(t) + \xi(t), \tag{3.2}$$

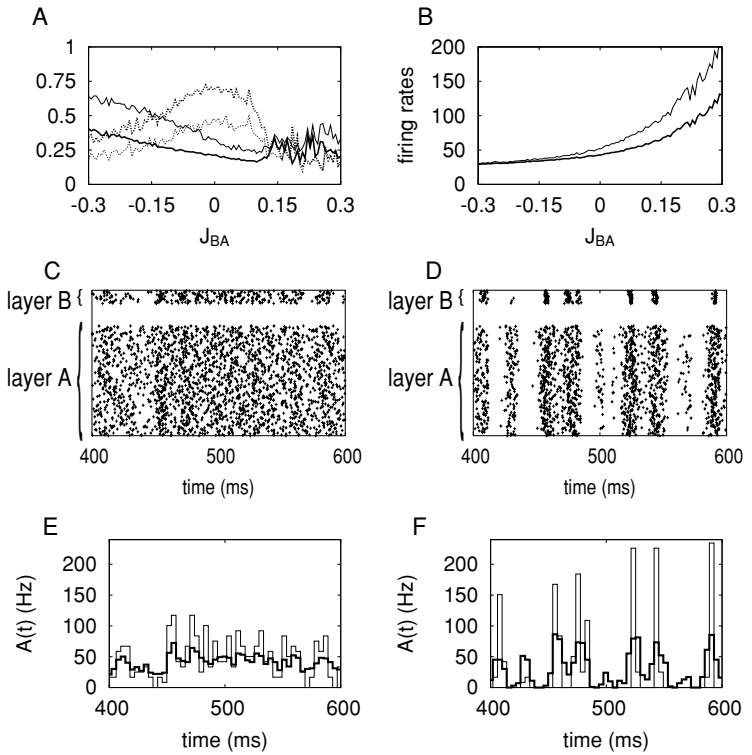

Figure 2: (A) Degree of synchrony (r, solid lines) and performance of the population rate coding (*corr*, dotted lines) in layers A (thick lines) and B (thin lines) when the strength of global feedback is varied. (B) Mean firing rates of single neurons in layer A (thick line) and ones in layer B (thin line). Examples of raster plots of excitatory neurons (lower traces) and inhibitory neurons (upper traces) are also shown for (C) $J_{BA} = 0$ and (D) $J_{BA} = -0.25$. (E, F) The normalized population firing rates $A(t)$ for the population of excitatory neurons (thick lines) and that of inhibitory neurons (thin lines), calculated with bin width 4 ms. E and F correspond to C and D, respectively.

where $\xi(t)$ is a white gaussian process with standard deviation 1, $I_0 = 1.4$ is the input bias, $C = 5$ is the strength of input modulation, and τ_{OU} is assumed to be 10 ms. We also set $w = 2.5$ ms in equation 2.3, $\tau_{BA} = 30.0$ ms, and $\sigma = 0.08$.

The degree of synchrony and the performance of the population rate coding are shown in Figure 2A as functions of the feedback strength. In the purely feedforward situation with $J_{BA} = 0$, less synchrony and larger values of *corr* are observed compared with when $J_{BA} < 0$. As J_{BA} tends more negative, the synchronous mode is first seen. Then as it increases toward

zero, asynchrony with high resolution of the population rate code gradually appears (Masuda & Aihara, 2002b, 2003a; van Rossum et al., 2002; Litvak et al., 2003). A more negative feedback gain provides the neurons in layer A with more correlated inputs in the form of common spike trains from layer B. Then layer A is forced to synchronize more strongly (Damasio, 1989; Sillito et al., 1994; Murphy et al., 1999; Doiron et al., 2003; Masuda & Aihara, 2003a), and the enhanced synchrony in turn supplies more correlated feedforward inputs to layer B to induce synchrony there as well (Abeles, 1991; Diesmann et al., 1999; Câteau & Fukai, 2001; van Rossum et al., 2002; Masuda & Aihara, 2003a; Litvak et al., 2003; Reyes, 2003). The results are consistent with the general tendency that reduced firing rates reinforce synchrony in recurrent networks (Brunel & Hakim, 1999; Burkitt & Clark, 2001), since the negative global feedback in our network obviously decreases firing rates. Figures 2C (for $J_{BA} = 0$) and 2D (for $J_{BA} = -0.25$) show example raster plots of $n_1 = 250$ neurons in layer A (lower traces) and $n_2 = 30$ neurons in layer B. These figures, together with the time-dependent firing rates shown in Figures 2E and 2F corresponding to Figures 2C and 2D, respectively, support that there is a transition between synchronous and asynchronous regimes as explained above. At the same time, oscillatory activities, which are our interest, are evident, particularly in the presence of delayed feedback (see Figure 2D). What mechanisms underlie such oscillations and how oscillations are related to information coding are examined in sections 4, 6, and 7. As a remark, the use of $J_{BA} < 0$ can obscure the biological sense of the neurons in layer B, because they send inhibitory spikes to layer A and excitatory spikes to layer B. However, the results are qualitatively the same even if the coupling within layer B is inhibitory (data not shown).

The observables from layer B roughly approximate those from layer A for all J_{BA} since the dynamics in layer B is correlated to that in layer A (Brunel, 2000; Laing & Longtin, 2003; see Figure 2). This is consistent with experimental evidence in, for example, the visual system (Billock, 1997) and the hippocampus (Klausberger et al., 2003). More precisely, the amount of information on $I(t)$ in layer B is limited by that in layer A. Consequently, in layer B, larger r and smaller *corr* than in layer A are always observed. For this reason, we do not show *corr* and r of layer B in the following figures.

Figure 2A indicates that for $J_{BA} > 0$, significant synchrony is not established. This is so even though synchrony is expected at higher J_{BA}, which produces more correlated input to layer A. Noise is amplified through the positive feedback loop, and Figure 2B shows that firing rates are drastically increased as a function of J_{BA}. The combined effects give rise to a tendency toward asynchrony (Brunel & Hakim, 1999; Burkitt & Clark, 2001), which seems to override the synchronizing effect of the correlated inputs. In contrast to the switching between the synchronous mode and the population rate code mode obtained for negative feedback, *corr* decreases and r does not robustly increase as J_{BA} goes positive large. As mentioned, the positive

feedback elicits autonomous autocatalytic reverberation even after external inputs are removed. Then firing rates just saturate at large values so that the network behavior is almost ignorant of the input information, deteriorating the population rate coding (Douglas et al., 1995). This consequence is also likely for more elaborated conductance-based neuron models and real neurons since saturating effects with monotonic frequency-input (f-I) curves are observed in these cases as well (Hô & Destexhe, 2000; Chance, Abbott, & Reyes, 2002). Although nonmonotonic f-I relations because of conductance dynamics (Kuhn, Aertsen, & Rotter, 2004) possibly change our conclusions, we concentrate on more conventional cases. To put all the cases of J_{BA} together, the purely feedforward architecture with $J_{BA} = 0$ naturally maximizes *corr* since *corr* measures the performance of the simplest task of mimicking inputs.

Although signal amplification and maintenance of high firing rates are achieved by positive feedback loops (Douglas et al., 1995), positive feedback is often harmful (e.g., seizure), and it is also inefficient in terms of the consumed power (Knight, 2000). Positive feedback must be used in more local or specific manners. For example, it may activate certain parts of a network for particular functions to be turned on, or for a specific aspect of stimuli to be magnified, as suggested by the experiments in the electric fish circuitry (Berman & Maler, 1999).

4 Bandpass Filtering of Dynamic Inputs

In this section, we investigate how the interplay of various factors with different timescales influences information processing. To this end, let the external inputs be the sinusoidal waveforms represented by

$$I(t) = I_0 + C \sin(2\pi f_{ext} t), \tag{4.1}$$

where I_0 and C are the bias and the amplitude of modulation, respectively. The relevance of sinusoidal inputs to biological neural systems has been explained in section 1. We vary w in equations 2.3 and 2.4 according to $w = 100/f_{ext}$ ms so that the resolution of discretizing $I(t)$ into $\{s_1(i)\}$ is independent of the timescale.

As to the modulation strength, there is always competition between f_{ext} and inherent stochastic dynamics of single neurons (Longtin, 1995) or that of networks, as we will see. Obviously, *corr* increases with C at first, meaning that stronger modulation more easily facilitates better population rate coding with some, but not perfect, phase locking (Burkitt & Clark, 2001). If C is even stronger, *corr* degrades to some extent because of almost perfect phase locking, which disregards the detailed temporal structure of $I(t)$. In these situations, the contribution of the neural network dynamics is negligible, and abundant results for single neurons or neural networks without

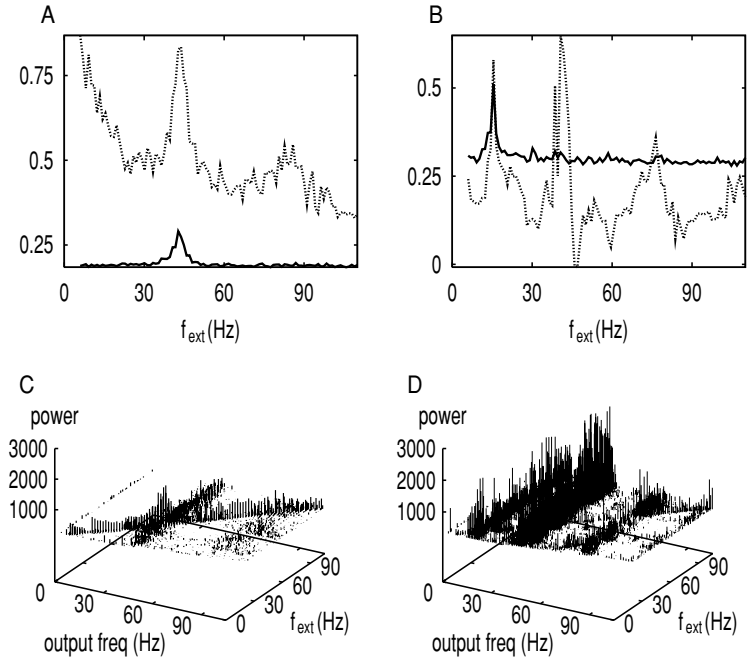

Figure 3: (A, B) The degree of synchrony (r, solid lines) and the performance of the population rate coding (*corr*, dotted lines) of layer A. (C, D) Power spectra of the population firing rates of layer A. For clarity, only the values of power more than 100 are plotted. We set $I_0 = 1.4$ and $\tau_{BA} = 30.0$ ms. The dependence on f_{ext} is examined for $J_{BA} = 0$ (A, C) and $J_{BA} = -0.25$ (B, D).

global feedback support that firing times are regulated by the peaks of external inputs without regard to network interactions (Gerstner et al., 1996; Longtin & St-Hilaire, 2000; Masuda & Aihara, 2003b). However, here we examine the regime in which the dynamics are not so strongly entrained by inputs. We set $C = 0.10$, which is small compared with values of I_0 used in sections 4.1 and 4.2.

4.1 Effects of Global Feedback

4.1.1 Feedforward Only First, a purely feedforward architecture is contrasted with one with global feedback, with which we are concerned. We set $\tau_{BA} = 30$ ms, $I_0 = 1.4$, and $\sigma = 0.07$. The coding profiles of layer A dependent on f_{ext} are shown in Figure 3A for $J_{BA} = 0$. Compared with the case in which $J_{BA} = -0.25$ (see Figure 3B), the level of synchrony is lower and *corr* is larger for most of the range of the input frequency. This agrees with the results in section 3. However, peaks of *corr* and r appear simultaneously

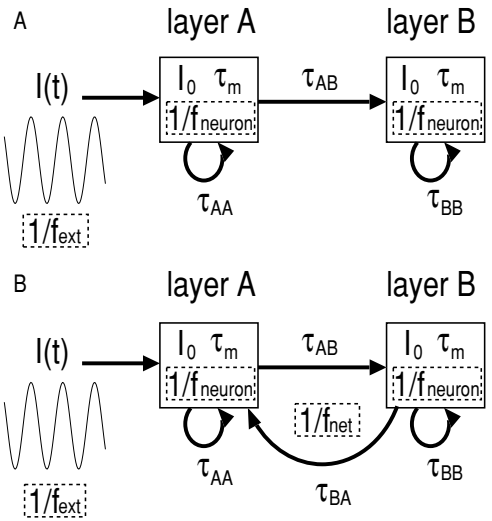

Figure 4: Schematic figure showing how f_{ext}, f_{neuron}, and f_{net} are set when the feedback loop is (A) absent and (B) present.

at $f_{ext} \cong 42$ Hz and its harmonics. Generally, spiking neurons have inherent output frequencies for a constant input (Knight, 1972, 2000; Rinzel & Ermentrout, 1998; Wilson, 1999; Lindner & Schimansky-Geier, 2002; Izhikevich et al., 2003). With the values of τ_m and I_0 given above, each LIF neuron in open loop has the characteristic resonant frequency f_{neuron} (see Figure 4A), which is about 42 Hz. Better phase locking and better population rate coding of inputs are realized when f_{ext} is approximately equal to f_{neuron} or its harmonics (Knight, 1972, 2000; Hunter et al., 1998; Longtin, 2000; Klausberger et al., 2003; Buzsáki & Draguhn, 2004). Figure 3 can also be regarded as an inverted tuning curve showing the input amplitudes necessary to achieve a certain level of *corr*. The resonant regimes require just small input amplitudes for locking, population rate coding with high resolution, and presumably synchrony.

The simultaneous increase in *corr* and r in the resonant scheme seems contradictory to the trade-off between synchrony and efficiency in population rate coding realized by asynchrony. However, what happens is the locking of spikes onto the peaks of $I(t)$. Even if the neurons fire only around the peaks of $I(t)$, firing rates approximate the sinusoidal inputs well enough to result in large *corr*. At the same time, the phase locking leads to synchronization, which yields r even larger than the case of sinusoidally modulated firing rates. The power spectra of the population firing rates of layer A are shown in Figure 3C for changing f_{ext}. We verify that oscillations are enhanced around the resonant frequencies. This is consistent with the fact

that an oscillation of population activities always accompanies some degree of synchrony (Brunel, 2000).

On the other hand, Figure 3C indicates that the effect of f_{ext} and that of f_{neuron} on the output frequency compete with each other in nonresonant situations, resulting in relatively irregular and asynchronous firing. However, asynchrony in this case does not mean efficient population rate coding (see Figure 3A). Firing times are not entirely locked to the stimulus peaks but determined as a compromise between the input and the intrinsic neuronal-network dynamics. Accordingly, the purely feedforward networks filter away the temporal information on nonresonant inputs. This mechanism of bandpass filtering is commonly found in suprathreshold and subthreshold regimes (Knight, 1972, 2000; Longtin & St-Hilaire, 2000; Longtin, 2000; Lindner & Schimansky-Geier, 2002).

4.1.2 Negative Feedback. Let us discuss dynamics of networks with negative global feedback. Analytical results based on analog neurons (Marcus & Westervelt, 1989; Longtin, 1991; Giannakopoulos & Zapp, 1999; Wilson, 1999; Laing & Longtin, 2003) and neural populations with exact threshold dynamics (Brunel & Hakim, 1999; Brunel, 2000) show that another inherent frequency appears via the Hopf bifurcation as $-J_{BA}$ or τ_{BA} increases. This new frequency f_{net} is introduced by the delayed global feedback loop, as schematically shown in Figure 4B. The coding profiles for $J_{BA} = -0.25$ are shown in Figures 3B and 3D. With this J_{BA}, a limit cycle corresponding to the oscillatory population firing rates exists, and the network has two characteristic frequencies, $f_{neuron} \cong 40$ Hz and $f_{net} \cong 15$ Hz. We note that f_{neuron} is smaller than the purely feedforward case because of the net negative feedback inputs to layer A (Douglas et al., 1995). We observe in Figure 3B larger values of *corr* and r near $f_{ext} = f_{net}$, as well as near $f_{ext} = f_{neuron}$. Also, *corr* is raised near the harmonics of f_{neuron}. Figure 3D supports the notion that the enhanced synchrony and the better population rate coding are accompanied by reinforced regular oscillations and phase locking around resonant frequencies. For nonresonant inputs, the peaks in *corr*, r, and the power spectra disappear as a result of competition between f_{ext}, f_{neuron}, and f_{net}.

The coexistence of two characteristic frequencies f_{net} and f_{neuron} can be understood with an analysis of the population firing rates depending on the parameter J_{BA}. Here we explain it qualitatively; more detailed analyses on the Hopf bifurcation are provided in section 7. Let us suppose for simplicity that $I(t)$ is a constant bias plus some noise and that J_{BA} decreases from 0. At low $|J_{BA}|$, constant firing rates corresponding to totally asynchronous population activities are the stable fixed points, if intralayer coupling is ignored. However, the neurons fire more or less synchronously even at this stage because of nonzero J_{BA}. Therefore, the constant firing rates can be interpreted as somewhat synchronous firing with output frequency f_{neuron} (see Figure 4A). Past the Hopf bifurcation point, f_{neuron} changes continuously

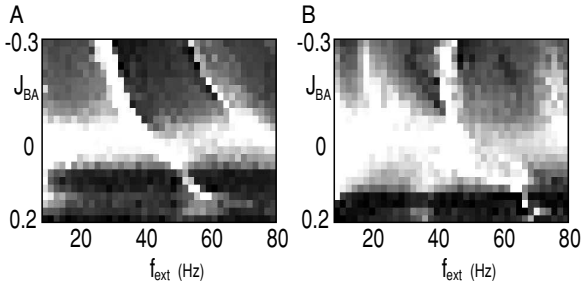

Figure 5: Dependence of *corr* on J_{BA} and f_{ext} with (A) $\tau_{BA} = 20.0$ ms and (B) $\tau_{BA} = 30.0$ ms. We set $I_0 = 1.4$. Brighter points correspond to larger values of *corr*.

and begins to oscillate in time at the eigenmode corresponding to f_{net} (see Figure 4B).

The inverse of the resonant frequency f_{net} is approximated by twice the loopback time: $2\tau_{BA} = 60 \cong 1/0.017$ ms since the feedforward synaptic delay and the response time of the neural populations (Knight, 1972; Gerstner & Kistler, 2002) are much smaller than τ_{BA} in our framework and many others. This agrees with the analytical calculations in section 6 based on linear response theory and is intuitively understood as follows (Brunel & Hakim, 1999). In response to increasing firing rates in layer A, strong negative feedback reverberates into layer A approximately after τ_{BA}. Then the firing rates in layer A decrease to make layer B less activated. The strong inhibition in layer A imposed by the negative feedback is removed after another τ_{BA}, which completes one round. This is numerically confirmed (Doiron et al., 2003; Maex & De Schutter, 2003), and theoretical results also guarantee that $1/f_{net}$ falls somewhere in $[2\tau_{BA}, 4\tau_{BA}]$ depending on situations (Brunel & Hakim, 1999; Giannakopoulos & Zapp, 1999; Laing & Longtin, 2003; Doiron et al., 2004).

Next, we examine the influence of J_{BA} on input filtering more systematically. The values of *corr* for various values of J_{BA} and f_{ext} are shown in Figures 5A and 5B for $\tau_{BA} = 20$ ms and $\tau_{BA} = 30$ ms, respectively. We have set $I_0 = 1.4$ and $\sigma = 0.02$. Since the dynamical states are kept more or less synchronous and r does not give us as much information as *corr* does, we show only the values of *corr* in Figure 5 and later in Figure 6. Black and white regions correspond to $corr \cong 0$ and $corr \cong 1$, respectively. Near $J_{BA} = 0$, only feedforward filtering is in operation, and it is broadly tuned. Although it has a lowpass property whose cutoff frequency is specified by the membrane constant, the bandpass cutoff is not seen in the numerical results because the cutoff frequency is very high. Near $J_{BA} = -0.05$, oscillatory network dynamics begin to be observed, presumably corresponding to the Hopf bifurcation assessed with $\sigma = 0$. Then, only the inputs whose

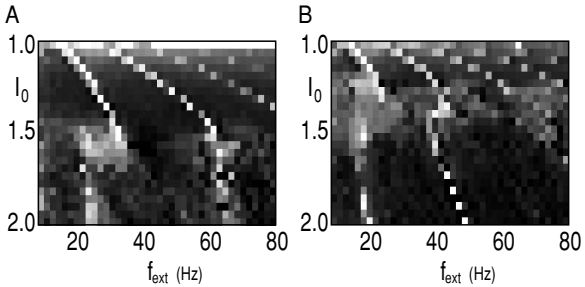

Figure 6: Dependence of *corr* on I_0 and f_{ext} with (A) $\tau_{BA} = 20.0$ ms and (B) $\tau_{BA} = 30.0$ ms. We set $J_{BA} = -0.25$. Brighter points correspond to larger values of *corr*.

f_{ext}'s are resonant with f_{net} or f_{neuron} are readily transmitted, and this feedback bandpass filtering is sharply tuned. As expected, f_{net} changes from approximately 25 Hz to 15 Hz as we vary τ_{BA} from 20 ms to 30 ms. For positive J_{BA}, oscillatory synchrony is actually difficult to build up, as we mentioned above. Analytical results also suggest that population firing rates do not oscillate but are constant for small but positive J_{BA} (Knight, 2000; Laing & Longtin, 2003). On the other hand, the peaks associated with f_{neuron} and its harmonics persist up to a larger positive $J_{BA} \cong 0.15$, where $f_{neuron} \cong 55$ (resp. 65) Hz in Figure 5A (resp. Figure 5B). Both f_{net} and f_{neuron} increase in J_{BA}. However, f_{neuron} is more sensitive to J_{BA}, since J_{BA} directly affects the level of effective bias (Maex & De Schutter, 2003). Another point is that *corr* generally decreases as $|J_{BA}|$ increases, consistent with Figure 2A.

4.2 Effects of Input Bias. In addition to the principal oscillatory component of inputs, an input bias is perpetually subject to changes. With $J_{BA} = -0.25$ and $\sigma = 0.03$ fixed, values of *corr* for varying I_0 and f_{ext} are numerically calculated. Figures 6A and 6B correspond to $\tau_{BA} = 20$ ms and $\tau_{BA} = 30$ ms, respectively. The neuronal frequency f_{neuron} is identified by the brighter regions with larger *corr*, which mark the resonance between f_{ext} and f_{neuron}. In Figures 6A and 6B, they are relatively bright oblique regions touching $f_{ext} \cong 50$ Hz at $I_0 = 2.0$. Similarly, resonant peaks corresponding to f_{net} are those touching $f_{ext} \cong 25$ (resp. 15) Hz at $I_0 = 2.0$ in Figure 6A (resp. Figure 6B). Also some harmonics of f_{neuron} and f_{net} are observed as oblique bands. At first sight, f_{neuron} increases with I_0 in a smooth manner. This property, also suggested in section 4.1, is reminiscent of the property of class I neurons (also called type I membranes) or of LIF neurons (Knight, 1972; Rinzel & Ermentrout, 1998; Masuda & Aihara, 2002a). In contrast, the peak associated with f_{net} does not move that much, because the frequency of the network oscillation caused by the Hopf bifurcation is rather insensitive to the bias, even well beyond the bifurcation point (Rinzel & Ermentrout,

1998; Masuda & Aihara, 2002a; Izhikevich et al., 2003). These results agree with the analytical results in section 6 and are discussed in more detail in section 8.

In summary, there are two oscillation periods. The intrinsic neuron timescale f_{neuron} is susceptible to I_0 and J_{BA}, whereas the intrinsic network timescale f_{net} depends much on τ_{BA} and to some extent on J_{BA}. The latter oscillation is observed only when negative feedback is large enough. When the input timescale f_{ext} matches either f_{neuron} or f_{net}, both input-output correlation and network synchrony increase, and the network bandpasses sinusoidal inputs.

5 Spike Response Model

To take a closer look at the mechanism of bandpass filtering, we introduce the description on population activities based on a simplified spike response model (SRM) (Gerstner & Kistler, 2002). The SRM is equipped with realistic features of neurons such as spiking mechanisms, stochasticity, and refractory periods. At the same time, it allows exact treatments of delay-induced synchronous network oscillations and oscillations of single neurons. Based on the SRM, we derive linear frequency response functions in section 6 and bifurcation diagrams in section 7. In this section, we briefly explain the formulations necessary for sections 6 and 7. However, we move the mathematical details to appendix A since the calculations are basically the same as those in Gerstner and Kistler (2002). Our novel point is the consideration of delayed feedback. For complete derivation, also refer to Doiron (2004).

Let us assume a single-layered recurrent network with feedback delay τ_d. This reduction from the network with two layers is justified for a moment by the mathematical fact that the dynamics of layer B is enslaved by that of layer A in the sense that their firing rates are locked with a phase lag (Brunel, 2000; Laing & Longtin, 2003; Doiron et al., 2003, 2004).

After some calculations as shown in appendix A, we obtain a delay differential system involving the effective input potential $h(t)$ and the population firing rate $A(t)$:

$$h(t) = \int_0^\infty \mathrm{e}^{-s/\tau_m} \times \left(J \int_{-\infty}^{\infty} \mathcal{G}_{\sigma_1}(r') A(t - s - \tau_d - r') dr' + I(t - s) \right) ds, \quad (5.1)$$

and

$$A(t) = \frac{f[h(t)]}{1 + \tau_r f[h(t)]} \equiv g[h(t)]. \quad (5.2)$$

Here J is the uniform feedback gain, τ_r is the absolutely refractory period, $\mathcal{G}_{\sigma_1}(r')$ is the noise kernel to account for the stochasticity in the dynamics, and f given in equation A.10 in appendix A implements a stochastic spiking

mechanism with threshold. We remark that we now use the letter A for population activity, not to be confused with a layer label. Equation 5.2 dictates that a firing rate is determined by monotonic nonlinear function of $h(t)$. In turn, $h(t)$ comprises the filtered versions of the neural activity reverberating with delays and the external input. The lowpass filtering stems from the membrane time constant of the single neuron, namely, τ_m.

6 Resonance Conditions Based on Linear Response Theory

In this section, we derive the linear response function in the frequency domain to examine the resonance conditions. We again follow the previous work (Knight, 1972, 2000; Gerstner, 2000; Gerstner & Kistler, 2002) except that we take into account the delayed feedback. This analysis is qualified because in section 4, we worked out the numerical simulations with the weak input modulation.

For the inputs given in equation 4.1 with small C, let the population firing rates be

$$A(t) = \overline{A} + \Delta A(t), \tag{6.1}$$

where $\overline{A}$ is the mean firing rate. For simplicity, we set $\tau_r = 0$ in this section. We also apply the deterministic firing rule without long memory, by replacing $h(t)$ with $h(t|\hat{t})$ in equation A.9 and assuming $\beta \to \infty$ in equation A.10. Instead, we introduce the reset noise (Gerstner, 2000; Gerstner & Kistler, 2002), which is more mathematically tractable for the purpose of deriving frequency response functions. The reset noise causes the jitter in the reset time in the form of the gaussian distribution with variance σ_2^2. Then, in terms of h, the dynamical equation for the population firing rates linearized around the stationary rate $\overline{A}$ becomes

$$\begin{aligned}\Delta A(t) = &\int_{-\infty}^{\infty} \mathcal{G}_{\sigma_2}(r)\Delta A(t - T_0 - r)dr \\ &+ \frac{\overline{A}}{v'(\theta)}\left(h'(t) - \mathrm{e}^{-T_0/\tau_m}\int_{-\infty}^{\infty}\mathcal{G}_{\sigma_2}(r)h'(t - T_0 - r)dr\right),\end{aligned} \tag{6.2}$$

where T_0 is the backward interspike interval that is almost equal to an interspike interval $1/f_{neuron}$, and $v'(\theta) > 0$ is the rate of increase in the membrane potential v at the threshold $v = \theta$, which we assume to be constant (Gerstner & Kistler, 2002). By applying the Fourier transform to equations 5.1 and 6.2, we obtain the following equations for the radial frequency $\omega \neq 0$:

$$\hat{h}(\omega) = \frac{\tau_m}{1 + i\omega\tau_m}\left(J\,\hat{\mathcal{G}}_{\sigma_1}(\omega)\mathrm{e}^{-i\omega\tau_d}\hat{A}(\omega) + \hat{I}(\omega)\right), \tag{6.3}$$

$$\hat{A}(\omega) = \hat{\mathcal{G}}_{\sigma_2}(\omega)\hat{A}(\omega)\mathrm{e}^{-i\omega T_0} + \frac{\overline{A}}{v'(\theta)}\left(\hat{h}'(\omega) - \mathrm{e}^{-T_0/\tau_m - i\omega T_0}\hat{\mathcal{G}}_{\sigma_2}(\omega)\hat{h}'(\omega)\right), \quad (6.4)$$

where the Fourier transform of a function is denoted by putting $\hat{}$. The Fourier transform of the gaussian distribution is given by

$$\hat{\mathcal{G}}_{\sigma'}(\omega) = \exp\left(-\frac{\sigma'^2\omega^2}{2}\right). \quad (6.5)$$

Combining equations 6.3 to 6.5, we derive the frequency response function in the following form:

$$\frac{\hat{A}(\omega)}{\hat{I}(\omega)} = \frac{\overline{A}\hat{F}(\omega)}{v'(\theta)} \Bigg/ \left(1 - \exp\left(-\frac{\sigma_2^2\omega^2}{2} - i\omega T_0\right) - \frac{\overline{A}\hat{F}(\omega)}{v'(\theta)} J \exp\left(\frac{-\sigma_1^2\omega^2}{2} - i\omega\tau_d\right)\right), \quad (6.6)$$

where

$$\hat{F}(\omega) = \frac{i\omega\tau_m}{1 + i\omega\tau_m}\left(1 - \exp\left(-\frac{\sigma_2^2\omega^2}{2} - i\omega T_0 - \frac{T_0}{\tau_m}\right)\right). \quad (6.7)$$

We then ignore the term $\overline{A}/v'(\theta)$ in the numerator, which is independent of ω, and define the effective coupling strength by $\overline{J} = J\,\overline{A}/v'(\theta)$.

Figure 7 shows the gain function calculated as the absolute value of equation 6.6 for some parameter sets. In the resonant situations, $\mathrm{e}^{-i\omega T_0}$ or $\overline{J}\,\mathrm{e}^{-i\omega\tau_d}$ are more or less maximized to make the denominator of equation 6.6 small (Knight, 2000; Gerstner & Kistler, 2002). The change in T_0 mainly affects the second term of the denominator, whereas τ_{BA} and J_{BA} influence the third term. For $(T_0, \overline{J}, \tau_d) = (25\text{ ms}, -0.5, 30\text{ ms})$, the response gain (solid lines in Figure 7) actually has three peaks: at $f_{net} \cong (2\tau_d)^{-1} = 18$ Hz, $f_{neuron} \cong T_0^{-1} = 40$ Hz, and $2\,f_{neuron}$ (also see Figure 4B). Figure 7A shows that if we remove the global feedback, the peak at f_{net} vanishes with little influence on the peaks at f_{neuron} and $2\,f_{neuron}$ (also see Figure 4A). With $J < 0$ present, only the former peak shifts as we change τ_d, as shown in Figure 7B. By contrast, Figure 7C shows that the latter peaks mainly move as we vary T_0, which is sensitive to the input bias. As a remark, the nonlinear bifurcation theory in section 7 and others (Marcus & Westervelt, 1989; Longtin, 1991; Giannakopoulos & Zapp, 1999; Wilson, 1999) claims that the feedback delay must be large enough to produce a Hopf bifurcation with the network oscillation. This is not covered by the linear theory developed here. On the other hand, the resonant peak at f_{net} may be identified even in the subthreshold regime due to noise.

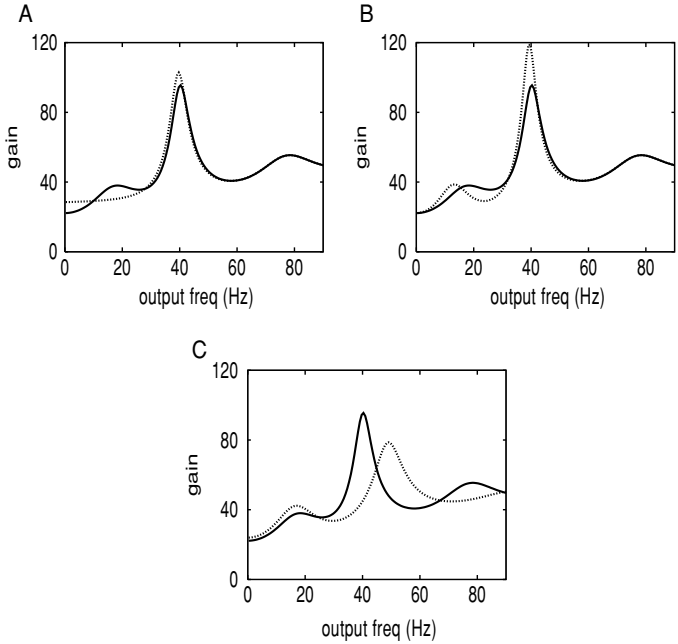

Figure 7: The gain functions for $T_0 = 25$ ms, $\overline{J}_0 = 0.5$, $\tau_d = 30$ ms (solid lines in (A), (B), and (C)) compared with $T_0 = 25$ ms, $\overline{J}_0 = 0$, $\tau_d = 30$ ms (dotted line in *A*), $T_0 = 25$ ms, $\overline{J}_0 = 0.5$, $\tau_d = 40$ ms (dotted line in *B*), and $T_0 = 20$ ms, $\overline{J}_0 = 0.5$, $\tau_d = 30$ ms (dotted line in *C*). We set $\sigma_1 = 8.0$ and $\sigma_2 = 4.0$.

We are in a position to explicitly take two layers into account. For simplicity, the intralayer coupling is ignored. After similar calculations that are detailed in appendix B, we end up with the frequency response function equation B.3. Essential points suggested by the denominator of equation B.3 are that f_{neuron} does not change with the consideration of two layers and that f_{net} is modified to $2(\tau_{AB} + \tau_{BA})^{-1}$, which is again twice the loopback time. More generally, we deal with the frequency response of N assemblies in appendix B. With these assemblies denoted by 1, 2, ..., N, the resonance frequency for a negative feedback loop of chain length k is given by

$$f_{net} = \frac{1}{2\left(\tau_{\rho_1\rho_2} + \tau_{\rho_2\rho_3} + \ldots + \tau_{\rho_k\rho_1}\right)}, \tag{6.8}$$

where $\{\rho_1, \ldots, \rho_k\}$ is an ordered subset of $\{1, 2, \ldots, N\}$.

On the other hand, f_{net} associated with a positive loop is not likely to be observed because the Hopf bifurcation points, which mark the emergence of oscillations (see section 7), are not crossed and positive feedback usually introduces instability (Knight, 2000). In reality, a pair of layers is not

necessarily interconnected, and the parameters differ for each loop. Among them, the contribution of the feedback loops with small $\tau_{\rho_1\rho_2} + \tau_{\rho_2\rho_3} + \ldots + \tau_{\rho_k\rho_1}$ and negative large effective gains ($\overline{J}_{\rho_1\rho_2}\overline{J}_{\rho_2\rho_3}\ldots\overline{J}_{\rho_k\rho_1}$ in appendix B) relative to other loops dominates the summation in equation B.8. Only these loops effectively affect the bandpass properties. If the contribution of the feedback loops to the denominator is small relative to one of the single-neuron dynamics ($(1 - \hat{\mathcal{G}}_{\sigma_2}e^{-i\omega T_0})^N$ in equation B.8), $f_{neuron} = 1/T_0$ is the only effective resonant frequency, and the network property is of feedforward or single-neuron nature.

To summarize, a feedback delay potentially sets an oscillation period distinct from one associated with a single-neuron oscillation. Actual appearance of the oscillation depends on whether the network has passed a Hopf bifurcation point, which is the topic of section 7.

7 Hopf Bifurcations in Network Activity

In this section, we show how a network oscillation occurs via a supercritical Hopf bifurcation in population activity. In biological terms, our results qualitatively clarify which network configuration accommodates oscillations that underlie enhanced coding of periodic inputs, as discovered in section 4. Theoretically, we characterize how oscillations emerge in the SRM supplied with a delayed feedback. This bifurcation is set by both the single-cell excitability and the network feedback strength. The nonlinear analysis developed here complements the linear analysis in section 6. We set $J < 0$ to discuss the emergence of stable synchronous and oscillatory firing presented in section 4.

With the limit $\sigma_1 \to 0$ and $\sigma_2 \to 0$, we can transform equation 5.1 into the following scalar delay differential equation (Gerstner & Kistler, 2002):

$$\tau_m \frac{dh}{dt} = -h(t) + J\, A(t - \tau_d) + I(t). \tag{7.1}$$

The advantage of these approximations and transformations is that the system given by equations 5.2 and 7.1 is more tractable than the original system of equations A.3 and A.7 in appendix A.

We give a dynamical system analysis of equations 5.2 and 7.1. To this end, we consider only the autonomous network and set $I(t) = I_0$. Inserting equation 5.2 in equation 7.1 and performing the transformation $h \to (h - I_0)/\theta$ and $t \to t/\tau_m$ gives the nondimensionalized system:

$$\frac{dh(t)}{dt} = -h(t) + \tilde{J}\,\tilde{g}[(h(t - \tilde{\tau}_d)], \tag{7.2}$$

where the new dimensionless parameters are defined by $\tilde{J} = J/\theta\tau_m$ and $\tilde{\tau}_d = \tau_d/\tau_m$. The population activity $A(t)$ is now determined by $\tilde{g}[h(t)]$ with $\tilde{g}$ given in equation 5.2, but τ_r and $f(t)$ are replaced by $\tilde{\tau}_r = \tau_r/\tau_m$ and

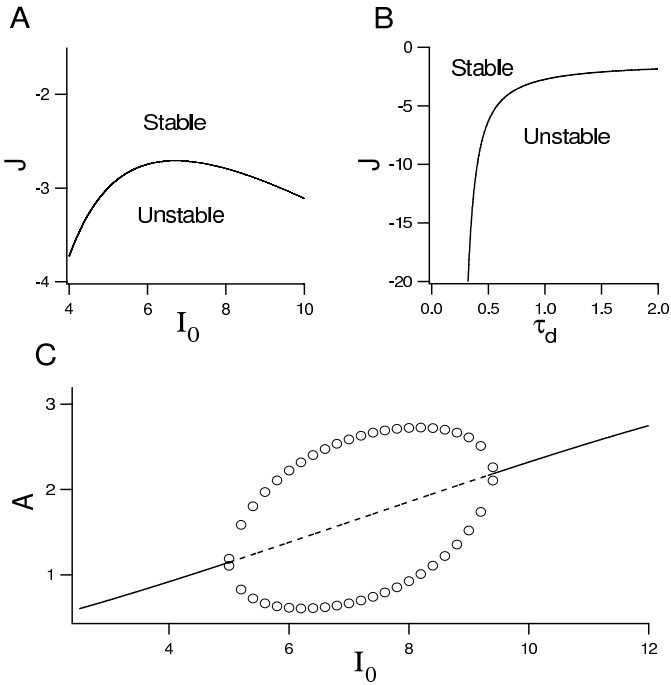

Figure 8: Hopf bifurcation in population dynamics. We integrate equation 7.2 with an Euler approximation scheme with a time step of 10^{-3}. The parameters are set at $\tau_r = 0.3$, $\beta = 1$, and $\tau_0 = 1$. (A) The bifurcation set Γ defines a curve of supercritical Hopf bifurcations in the J/I_0 parameter space. Equations C.1 and C.13 are solved using a bisection root-finding algorithm with a tolerance of 10^{-5}. The curve Γ computed for $\tau_d = 1$ partitions the parameter space into stable and unstable regimes, as labeled. (B) The Hopf bifurcation curve in the J/τ_d parameter space with $I_0 = 6$. (C) Bifurcation diagram for $A(t)$ with I_0 as a bifurcation parameter and $J = -3$. Solid lines and dashed lines represent stable and unstable fixed points, respectively. Open circles are the minimum and maximum of the oscillatory solution for $A(t)$ born out of the Hopf bifurcations.

$\tilde{f}(t) = \tilde{\tau}_0^{-1} \exp[\tilde{\beta}(h(t) + \tilde{I}_0 - 1)]$, respectively. We have set $\tilde{\beta} = \beta\theta$, $\tilde{I}_0 = I_0/\theta$, and $\tilde{\tau}_0 = \tau_0/\tau_m$.

In appendix C, we analyze equation 7.2 by numerically solving the transcendental characteristic equation caused by the delayed feedback. As a result, J/I_0 parameter space is partitioned into schemes. Figure 8A shows that the parameter space is divided into the stable regime where stationary firing rates are stable and the unstable regime where firing rates oscillate. The Hopf bifurcation occurs on the boundary curve denoted by Γ. As J varies, there is apparently only one Hopf bifurcation for a fixed I_0 (Marcus & Westervelt,

1989; Longtin, 1991; Brunel & Hakim, 1999; Brunel, 2000; Giannakopoulos & Zapp, 1999; Gerstner, 2000; Gerstner & Kistler, 2002; Laing & Longtin, 2003). Then an oscillation occurs for the negative feedback strength larger than a threshold. Actually, the situations of Figures 2C, 2E, 3A, 3C, and 4A correspond to the stable region in Figure 8A, whereas those of Figures 2D, 2F, 3B, 3D, and 4B correspond to the unstable region.

However, as I_0 grows, a stable network oscillation develops (Brunel & Hakim, 1999) and then is lost through a reverse Hopf bifurcation, which is also shown in the bifurcation diagram of $A(t)$ in Figure 8C. This is intuitively understood from the saturation of inhibitory feedback for large I_0 caused by the nature of $g(h)$. When inhibitory strength is saturated, large inputs can overtake any delay-induced oscillatory behavior. Figure 8B shows delay-induced instability in our population dynamics, consistent with other delayed dynamical systems (Marcus & Westervelt, 1989; Longtin, 1991; Brunel & Hakim, 1999; Giannakopoulos & Zapp, 1999; Wilson, 1999; Gerstner & Kistler, 2002). When J is larger negative, an oscillation begins with a smaller value of τ_d as τ_d increases.

In summary, larger $-J$ and τ_d with moderate I_0 are more in favor of network oscillations. Although oscillations can occur in a lot of ways in dynamical systems theory, the one here is through a Hopf bifurcation. Limit cycles that emerge from a Hopf bifurcation have rather stiff f_{net} compared with ones via, for example, a saddle-node bifurcation (Rinzel & Ermentrout, 1998). Such a rigid oscillation allows a strong resonance with a sinusoidal input to improve coding, as prominent in section 4. Effects of the type of bifurcation on coding performance are discussed in section 8.2.

8 Discussion

8.1 Relation to Experiments. Oscillatory synchrony is widely found on a diversity of relative timescales in various neural systems. In this section, we relate our results to experimental and relevant numerical results, particularly on sensory systems. Let us discuss neural systems separately according to the relative timescale f_{ext}/f_{neuron}.

Respiration provides external inputs with $f_{ext} \cong 1$ Hz $\ll f_{neuron}$. Oscillatory rhythm in olfactory systems can be locked to periodic respiratory inputs when they are present (Fontanini et al., 2003). Since oscillations are found even in the absence of inputs (Fontanini et al., 2003), olfactory systems are equipped with mechanisms to produce rhythms presumably owing to recurrent loops. Slow oscillations with frequency near f_{ext} are enhanced by respiration. Then built-in f_{net} may be close to actual respiration frequencies to enhance coding of general periodic inputs whose f_{ext} is close to respiration frequency. However, we note that much faster γ oscillations are ubiquitous in olfactory systems as well (Stopfer et al., 1997). In this case, inputs with larger f_{ext} may be relevant.

Similarly, hippocampal θ oscillations fall in this category if we consider that hippocampal neurons sense spike inputs or local field potentials from the θ rhythm as effective slow inputs. Such oscillatory field potentials may be caused by global feedback (Buzsáki & Draguhn, 2004). There, neurons typically fire more than once in a stimulus cycle around a specific phase of the periodic stimulus (Klausberger et al., 2003), reminiscent of the relation $f_{ext} \ll f_{neuron}$. The time constants associated with the intrinsic single neuronal dynamics are not important. Spike trains on top of θ oscillations are advantageous in accurate population rate coding. In addition, a subpopulation of neurons with these phase-locked spike trains may constitute a cell assembly for specific information processing (Buzsáki & Draguhn, 2004). The aforementioned results on olfactory systems are suggestive of the relation between f_{ext} and f_{net}, whereas those on the hippocampus particularly relate f_{ext} and f_{neuron}. They may be complementary to each other for understanding the interaction of the three timescales.

The other extreme $f_{ext} \gg f_{neuron}$ is found in auditory systems that are perpetually subject to sound inputs with high frequency (Gerstner et al., 1996). Electrosensory systems of weakly electric fish receive communication signals with relatively high frequency as well (Heiligenberg, 1991). These systems actually receive periodic forcing from the environments, hence directly fitting our framework. When $f_{ext} \gg f_{neuron}$, each neuron fires only sporadically with respect to the stimulus timescale. In the context of rate coding, a single neuron cannot encode these fast inputs. A population of neurons is called for to realize accurate rate coding (Shadlen & Newsome, 1998; Kistler & De Zeeuw, 2002; Masuda & Aihara, 2002b, 2003a; van Rossum et al., 2002). The fast input signals perhaps stem from some feedback loops with short delays. In this case, $f_{neuron} < f_{net}$ holds, as actually found in inferior olive neurons (Kistler & De Zeeuw, 2002) and in electrosensory networks (Doiron et al., 2003). Although we have mostly assumed $f_{neuron} > f_{net}$ in our analyses, the results can be extended to the case of $f_{neuron} < f_{net}$ without difficulty (Brunel & Hakim, 1999; Brunel, 2000).

Let us mention that superposition of different inputs can cause much smaller effective f_{ext}. For example, the electric fish interact by emitting amplitude-modulated electric fields into the water. Then oscillatory fields from many fish with various frequencies (several hundred cycles per second) are superposed (Heiligenberg, 1991). As a result, effective inputs to the fish are beating oscillations whose effective f_{ext} is, for example, the difference between two original f_{ext}. The fish may select the slow oscillatory components resonant with its f_{net} and/or f_{neuron}, possibly serving to identify specific individuals.

In visual systems, oscillatory field potentials with γ frequency (20–80 Hz) are ubiquitous and considered to be functionally relevant (Gray et al., 1989; Sillito et al., 1994; Ritz & Sejnowski, 1997; Murphy et al., 1999). Such oscillations do not originate from external visual inputs with γ frequency; effective f_{ext} or f_{ext}/f_{neuron} in this context seems unclear. Instead, they are

likely to be introduced by global feedback loops in the visual pathways such as thalamocortical networks (Sillito et al., 1994; Murphy et al., 1999; Destexhe & Sejnowski, 2003; Buzsáki & Draguhn, 2004). Then, in the sense of increased *corr* and r, the network is ready to select external inputs with frequency $f_{ext} \cong f_{net}$, where f_{net} is in the γ band.

As a general note, regular activities such as θ and γ oscillations are widely found in the brain. Consequently, chains of resonant signals may be propagated in neural networks, without allowing interference or participation of nonresonant signals (Izhikevich et al., 2003). If interspike intervals are sufficiently regular within each spike packet corresponding to one stimulus peak, as is the case for regular bursting, the coding performance of the network is also responsive to inputs fulfilling $f_{ext} \cong f_{neuron}$.

8.2 Difference in Two Types of Resonance. We have looked at the interplay between three characteristic frequencies—f_{neuron}, f_{net}, and f_{ext}—which are dependent, respectively, on the structure of intrinsic neural dynamics, network architecture, and the stimulus. When f_{ext} is close to f_{neuron} or its harmonics, oscillatory population firing rates read out f_{neuron} even for small signal amplitude. In this situation, the population rate coding with high temporal resolution, synchrony, regular oscillations, and strong but imperfect phase locking are realized at the same time. The magnitudes of J_{BA}, I_0, and also of τ_m mainly influence f_{neuron}. Stated in another way, the bandpass filtering associated with f_{neuron} is more adaptive in response to changes in I_0. This type of resonance is the same as that for single neurons (Knight, 1972, 2000; Hunter et al., 1998; Longtin, 2000; Klausberger et al., 2003).

When f_{ext} is close to f_{net}, oscillatory firing rates read out f_{net}. As shown in section 8, the Hopf bifurcation occurs with bifurcation parameter J_{BA} becoming more negative or τ_{BA} becoming larger. The resonant frequency f_{net} depends on τ_{BA} and J_{BA} (Marcus & Westervelt, 1989; Longtin, 1991; Brunel & Hakim, 1999; Giannakopoulos & Zapp, 1999; Wilson, 1999; Brunel, 2000; Gerstner, 2000; Laing & Longtin, 2003; Mehring et al., 2003; Doiron et al., 2004), but it is more robust against bias changes than are single-neuron oscillations.

To illustrate the inherent difference between single-neuron oscillations and network oscillations, let us first deal with a classification scheme of single-neuron dynamics. For single neurons, Hopf bifurcations can underlie the emergence of intrinsic oscillatory firing by class II neurons (also called type II membranes) such as the Hodgkin-Huxley neurons. Oscillatory class II neurons have f_{neuron} relatively robust against changes in parameters such as I_0. Consequently, they have bandpass properties, as our feedback networks do. Furthermore, they have other related functions, such as the rate coding of amplitude-modulated signals superposed on sinusoidal carriers (Longtin & St-Hilaire, 2000; Masuda & Aihara, 2003c).

On the other hand, class I neurons are essentially integrators or coincidence detectors and have distinct dynamical characteristics from those of class II neurons (Rinzel & Ermentrout, 1998; Wilson, 1999). The LIF neurons, which we have used, behave similarly to class I neurons, and their oscillations with frequency f_{neuron} are not robust. Actually, resonant peaks are extinguished for an increased level of noise ($\sigma = 0.10$) more easily than the resonant peaks at f_{net} and its harmonics (results not shown). Accordingly, such stable oscillations of class II neurons could be naturally associated with oscillatory activities abundant in experiments, as reviewed in section 1. However, there is an essential problem in these arguments in favor of active roles for class II neurons; most neurons in the mammalian brain, including pyramidal neurons and inhibitory interneurons, seem to be class I (Wilson, 1999) except, for example, some intrinsic oscillators in the frontal cortex of the guinea pig (Llinás et al., 1991) and some neurons similar to the squid giant neurons modeled by Hodgkin and Huxley (Aihara & Matsumoto, 1982).

Nevertheless, we find that class II properties persist at a network level. Networks with global feedback, or even those with local feedback whose delay is long enough to avoid inhibitory afterpotentials and refractory periods, have filtering as well as other properties of a single class II neuron. Furthermore, networks with global feedback have adaptive parameters such as J_{BA} related to learning. For example, the global feedback strength of the electric fish can be modulated even in a short time (Berman & Maler, 1999), possibly shifting f_{net} as well as f_{neuron}.

More generally, the feedback current gain J_{BA} used here should eventually be replaced by a feedback conductance that is voltage dependent and plastic (Douglas et al., 1995). This will likely endow neural networks with richer properties. Chains of these coherent oscillatory signals can also stably transmit from assemblies to assemblies (Knight, 2000; Masuda & Aihara, 2003c; Izhikevich et al., 2003). These functions are likely to be associated with the class II properties of network oscillations as well as those of single-neuron oscillations.

To summarize, synchrony, which is presumably relevant to information processing such as binding, normally yields decreased performance in the sense of rate coding (Masuda & Aihara, 2002b, 2003a; van Rossum et al., 2002; Litvak et al., 2003). However, in addition to the case in which $f_{ext} \cong f_{neuron}$, this law is violated when the delayed feedback creates f_{net} and f_{ext} is close to f_{net}. In these resonant situations, inputs are maximally transmitted with sharp tuning, synchrony, oscillations, and reliable rate codes. A final remark is that we have started with the SRM with realistic synaptic time courses. However, we have then restricted the models to current-input regimes for simplicity. Conductance-based synapses add another timescale that at least quantitatively changes dependence of f_{neuron} and f_{net} on other parameters (Hô & Destexhe, 2000; Chance et al., 2002). They can even yield a nonmonotonic relation between f_{neuron} and the input bias (Kuhn et al.,

2004), which may modify our results even qualitatively. A whole new study with different ratios of synaptic timescales is warranted for future work.

Appendix A: SRM for Neural Populations with Delayed Feedback

In this appendix, we explain the SRM model for neural populations with delayed feedback based on Gerstner and Kistler (2002) and Doiron (2004).

Let the population consist of n SRM neurons where the membrane potential of the ith neuron before next firing is given by

$$v_i(t) = \eta_i(t - \hat{t}) + h_i(t|\hat{t}), \tag{A.1}$$

where $\hat{t}$ is the last firing time. In equation A.1, $\eta_i(t)$ is a suitable refractory function, and $h_i(t|\hat{t})$ is the component of the membrane potential with $\hat{t}$ given, which is due to external inputs to the neuron. Equation A.1 is supplemented with a spiking rule: the jth spike time of neuron i, or $T_{i,j}$, is given by the jth time t such that $v_i(t) = \theta$, where θ represents the threshold value of membrane potential where generally nonlinear ionic currents produce action potentials. Typically, $\eta_i(t - \hat{t})$ is sufficiently negative for small $t - \hat{t}$ so as to effectively reset the membrane potential after spike discharge. With $T_{i,j}$, the population activity $A(t)$ is written by

$$A(t) = \frac{1}{n} \sum_{i=1}^{n} \sum_{j} \delta(t - T_{i,j}). \tag{A.2}$$

The actual population dynamics is a stochastic process because of various noise sources, such as the dynamical noise in equations 2.1 and 2.2. We first introduce noise caused by the jitter in the global feedback delay (Knight, 2000). It has the form of the gaussian distribution with variance σ_1^2. We denote the gaussian distribution with mean 0 and standard deviation σ_1 by $\mathcal{G}_{\sigma_1}$, and then the effective input potential defined by $h_i(t)$ in the presence of global feedback with delay τ_d is given by the following integral equation:

$$\begin{aligned} h_i(t) = J_i \int_0^\infty \epsilon_i(s) \int_{-\infty}^{\infty} \mathcal{G}_{\sigma_1}(r') A(t - s - \tau_d - r') dr' ds \\ + \int_0^\infty \kappa_i(s) I_i(t - s) ds, \end{aligned} \tag{A.3}$$

where J_i denotes the feedback gain for the ith postsynaptic neuron. Equation A.3 separates $h_i(t)$ into two parts. An external input $I_i(t)$ is convolved with a linear response kernel $\kappa_i(s)$. Network interactions are also expressed whereby the population activity $A(t)$ is convolved with a response kernel $\epsilon_i(s)$, which models both a synaptic and membrane response.

Since we consider homogeneous neural networks, we set $J_i = J, \eta_i(t) = \eta(t)$, $\epsilon_i(t) = \epsilon(t), \kappa_i(t) = \kappa(t)$, and $I_i(t) = I(t)$. All these conditions set our network to be a globally coupled network of identical neurons driven by a common stimulus. In the case of LIF neurons with its time course of the synaptic current given by the delta function, the response kernels are given by $\epsilon(t) = \kappa(t) = \tau_m^{-1} \mathrm{e}^{-t/\tau_m}$ $(t \geq 0)$, and the input potentials are connected by the relation

$$h(t|\hat{t}) = h(t) - h(\hat{t}) \exp\left(-\frac{t-\hat{t}}{\tau_m}\right). \tag{A.4}$$

Also using equation A.1, we obtain

$$h(t) = \int_0^\infty \mathrm{e}^{-s/\tau_m} \left(J \int_{-\infty}^\infty \mathcal{G}_{\sigma_1}(r') A(t-s-\tau_d-r') dr' + I(t-s) \right) ds, \tag{A.5}$$

which is equation 5.1, and

$$v(t) = \eta(t-\hat{t}) + \int_0^{t-\hat{t}} \mathrm{e}^{-s/\tau_m} \times \left(J \int_{-\infty}^\infty \mathcal{G}_{\sigma_1}(r') A(t-s-\tau_d-r') dr' + I(t-s) \right) ds. \tag{A.6}$$

For sufficiently simple model neurons without adaptive or bursting properties, such as the LIF neurons, the conservation law,

$$A(t) = \int_{-\infty}^t P_h(t|\hat{t}) A(\hat{t}) d\hat{t}, \tag{A.7}$$

holds in the limit $n \to \infty$. In equation A.7, $P_h(t|\hat{t})$ is the probability that a neuron with an input potential $h(t)$ fires at time $t > \hat{t}$. We supplement equation A.7 with the normalization condition:

$$\int_{-\infty}^t S(t|\hat{t}) A(\hat{t}) d\hat{t} = 1, \tag{A.8}$$

where $S(t|\hat{t})$ is the survivor function defined as the probability that a neuron does not emit a spike during the time interval $(\hat{t}, t)$. Equation A.8 simply states that all neurons have fired at least once over their history $(-\infty, t)$. Approximating the neuronal dynamics as a renewal process (Cox & Lewis, 1966), we can relate the interval distribution $P_h(t|\hat{t})$ to the hazard function

$f[h(t)]$ by

$$P_h(t|\hat{t}) = f[h(t)]S(t|\hat{t}) = f[h(t)]\exp\left(-\int_{\hat{t}}^{t} f[h(t')]dt'\right). \tag{A.9}$$

The hazard function $f[h(t)]$ may be conceived as a time-dependent firing probability; that is, a single cell emits a spike during the interval $(t, t + \Delta t)$ with probability $f[h(t)]\Delta t$. Equations 5.1 and A.7, in conjunction with an appropriate choice of $P_h(t|\hat{t})$, $\eta(t - \hat{t})$, and $f[h(t)]$, give a system of integral equations that determines network activities.

To derive a manageable delay differential system, we model a generally stochastic firing mechanism by adopting a noisy spike threshold. It is implemented by combining a standard spike escape rate and the hazard function in the form

$$f[h(t)] = \frac{1}{\tau_0}\exp(\beta(h(t) - \theta)). \tag{A.10}$$

Here β characterizes the threshold fluctuations. When $\beta \to \infty$, f is the Heaviside function centered at θ, providing a deterministic firing rule. In contrast, $\beta \to 0$ corresponds to a uniform and completely random firing probability of $1/\tau_0$ for all h. Next we choose our refractory function to be

$$\eta(t - \hat{t}) = \begin{cases} \infty, & (\hat{t} < t < \tau_r + \hat{t}) \\ 0, & (t \geq \tau_r + \hat{t}) \end{cases}, \tag{A.11}$$

meaning that the absolute refractory period is τ_r. The relative refractory period is not explicitly considered. Noting $P_h(t|\hat{t}) = 0$ for $\hat{t} < t < \hat{t} + \tau_r$, we derive from equations A.7, A.8, A.9, and A.11

$$A(t) = f[h(t)]\left[1 - \int_{t-\tau_r}^{t} A(t')dt'\right] = g[h(t)]. \tag{A.12}$$

This is the Wilson-Cowan equation (Wilson, 1999) for a population of neurons with only absolute refractoriness. If we further assume that both $I(t)$ and $A(t)$ vary on timescales much slower than τ_r, we can use a coarse graining of time to approximate equation A.12 as

$$A(t) = \frac{f[h(t)]}{1 + \tau_r f[h(t)]} = g[h(t)], \tag{A.13}$$

which is equation 5.2.

Appendix B: Frequency Response Functions of Layered Networks with Feedback

Let us assume that two layers A and B are connected with delays τ_{AB} and τ_{BA} and that the same value of T_0 is shared by layers A and B. The firing rate of layer A and that of B represented by $A_A(t) = \overline{A}_A + \Delta A_A(t)$ and $A_B(t) = \overline{A}_B + \Delta A_B(t)$, respectively, satisfy

$$\hat{A}_A = \hat{\mathcal{G}}_{\sigma_2} \hat{A}_A \mathrm{e}^{-i\omega T_0} + \hat{F} \overline{J}_{BA} \hat{\mathcal{G}}_{\sigma_1} \mathrm{e}^{-i\omega\tau_{BA}} \hat{A}_B + \frac{\overline{A}_A \hat{F}}{v'(\theta)} \hat{I}, \tag{B.1}$$

$$\hat{A}_B = \hat{\mathcal{G}}_{\sigma_2} \hat{A}_B \mathrm{e}^{-i\omega T_0} + \hat{F} \overline{J}_{AB} \hat{\mathcal{G}}_{\sigma_1} \mathrm{e}^{-i\omega\tau_{AB}} \hat{A}_A, \tag{B.2}$$

where $\overline{J}_{AB} \equiv J_{AB} \overline{A}_B / v'(\theta)$ and $\overline{J}_{BA} \equiv J_{BA} \overline{A}_A / v'(\theta)$ are the effective coupling strengths, and ω is omitted when possible. With equations B.1 and B.2, the frequency response function of layer A is written by

$$\frac{\hat{A}_A}{\hat{I}} = \frac{\frac{\overline{A}_A \hat{F}}{v'(\theta)} (1 - \hat{\mathcal{G}}_{\sigma_2} \mathrm{e}^{-i\omega T_0})}{\left(1 - \hat{\mathcal{G}}_{\sigma_2} \mathrm{e}^{-i\omega T_0}\right)^2 - \hat{F}^2 \overline{J}_{AB} \overline{J}_{BA} \hat{\mathcal{G}}_{\sigma_1}^2 \mathrm{e}^{-i\omega(\tau_{AB} + \tau_{BA})}}. \tag{B.3}$$

Let us next consider N assemblies labeled $1, 2, \ldots, N$. The transpose, the unit matrix of size N, and the firing rate of the ith assembly are denoted by T, E, and $A_i(t) = \overline{A}_i + \Delta A_i(t)$, respectively. We have

$$\hat{\mathbf{A}} = \hat{\mathcal{G}}_{\sigma_2} \mathrm{e}^{-i\omega T_0} \hat{\mathbf{A}} + \hat{F} \hat{\mathcal{G}}_{\sigma_1} X \hat{\mathbf{A}} + \frac{\overline{A}_1 \hat{F}}{v'(\theta)} \hat{\mathbf{I}}, \tag{B.4}$$

where

$$\hat{\mathbf{A}} = (\hat{A}_1, \hat{A}_2, \ldots, \hat{A}_N)^T, \tag{B.5}$$

$$\hat{\mathbf{I}} = (\hat{I}, 0, \ldots, 0)^T, \tag{B.6}$$

and X is an $N \times N$ matrix whose diagonal elements are zero and nondiagonal elements X_{ij} $(1 \le i, j \le N, i \ne j)$ are given by

$$X_{ij} = \overline{J}_{ji} \mathrm{e}^{-i\omega\tau_{ji}}. \tag{B.7}$$

Using equation B.4, the denominator of the frequency response function, which characterizes the resonant frequencies, can be expressed as follows:

$$
\begin{aligned}
&\det\left(\left(1-\hat{\mathcal{G}}_{\sigma_2}\mathrm{e}^{-i\omega T_0}\right)E-\hat{F}\hat{\mathcal{G}}_{\sigma_1}X\right)\\
&=\left(1-\hat{\mathcal{G}}_{\sigma_2}\mathrm{e}^{-i\omega T_0}\right)^N+\sum_{k=2}^{N}\left(1-\hat{\mathcal{G}}_{\sigma_2}\mathrm{e}^{-i\omega T_0}\right)^{N-k}\\
&\quad\cdot\sum_{(\rho_1\rho_2\ldots\rho_k)}\operatorname{sign}((\rho_1\rho_2\ldots\rho_k))\\
&\quad\times(-1)^k\hat{F}^k\hat{\mathcal{G}}_{\sigma_1}^k\overline{J}_{\rho_1\rho_2}\overline{J}_{\rho_2\rho_3}\ldots\overline{J}_{\rho_k\rho_1}\mathrm{e}^{-i\omega(\tau_{\rho_1\rho_2}+\tau_{\rho_2\rho_3}+\ldots+\tau_{\rho_k\rho_1})}\\
&=\left(1-\hat{\mathcal{G}}_{\sigma_2}\mathrm{e}^{-i\omega T_0}\right)^N-\sum_{k=2}^{N}\left(1-\hat{\mathcal{G}}_{\sigma_2}\mathrm{e}^{-i\omega T_0}\right)^{N-k}\\
&\quad\cdot\sum_{(\rho_1\rho_2\ldots\rho_k)}\hat{F}^k\hat{\mathcal{G}}_{\sigma_1}^k\overline{J}_{\rho_1\rho_2}\overline{J}_{\rho_2\rho_3}\ldots\overline{J}_{\rho_k\rho_1}\mathrm{e}^{-i\omega(\tau_{\rho_1\rho_2}+\tau_{\rho_2\rho_3}+\ldots+\tau_{\rho_k\rho_1})},
\end{aligned}
\tag{B.8}
$$

where the summations are over all the possible k cycles $(\rho_1\rho_2\ldots\rho_k)$ out of $\{1,2,\ldots,N\}$, and we have used the fact that the sign of a k cycle as a permutation is equal to $(-1)^{k-1}$. If the coupling is weak enough to prohibit equation B.8 from being negative, minimization of each term of the last summation in equation B.8 leads to equation 6.8, namely,

$$
f_{net}=\frac{1}{2\left(\tau_{\rho_1\rho_2}+\tau_{\rho_2\rho_3}+\ldots+\tau_{\rho_k\rho_1}\right)}
\tag{B.9}
$$

for a negative k cycle:

$$
\overline{J}_{\rho_1\rho_2}\overline{J}_{\rho_2\rho_3}\ldots\overline{J}_{\rho_k\rho_1}<0.
\tag{B.10}
$$

Appendix C: Bifurcation Analysis of Network Activity

In this appendix, we present the bifurcation analysis of equation 7.2. Hereafter we drop ˜ to simplify notation. Fixed points of equation 7.2, which are denoted by h^*, are given by the roots of the following transcendental equation:

$$
h^*=J\,g(h^*).
\tag{C.1}
$$

Because of the form of g, equation C.1 admits just one real root for all values of β, τ_0, $\tau_r>0$ and $J<0$. Linearizing about the fixed point yields the following local dynamics:

$$
\frac{dh(t)}{dt}=-h(t)+Dh(t-\tau_d),
\tag{C.2}
$$

where

$$D \equiv J \left.\frac{dg}{dh}\right|_{h=h^*} = \frac{J\beta \exp(\beta(h^* + I_0 - 1))\tau_0}{(\tau_0 + \tau_r \exp(\beta(h^* + I_0 - 1)))^2}. \tag{C.3}$$

Substituting the ansatz $h(t) = h_0 e^{\lambda t}$, where h_0 is a constant, into equation C.2 yields the characteristic equation:

$$\lambda + 1 - De^{-\lambda\tau_d} = 0. \tag{C.4}$$

Substitution of $\lambda = a + ib$ $(a, b \in \mathbb{R})$ into equation C.4 gives

$$a = De^{-\tau_d a}\cos(\tau_d b) - 1, \tag{C.5}$$

$$b = -De^{-\tau_d a}\sin(\tau_d b). \tag{C.6}$$

By considering the case when $a = 0$, we have from equations C.5 and C.6

$$1 = D\cos\tau_d b, \tag{C.7}$$

$$b = \sqrt{D^2 - 1}. \tag{C.8}$$

Since $b \in \mathbb{R}$, we have $|D| \geq 1$. The set of equations C.7 and C.8 admits a countably infinite number of solutions given by

$$b_k = \frac{1}{\tau_d}\left[\arccos\frac{1}{D_k} + 2\pi k\right], \tag{C.9}$$

$$D_k = \sqrt{b_k^2 + 1}, \tag{C.10}$$

with $k = 0, 1, 2, \ldots$. For each k, we have a pair of conjugate eigenvalues $\lambda_k = \pm ib_k$ that lie on the imaginary axis. We show that for each k, the dynamical system represented by equation 7.2 is at a Hopf bifurcation.

The Hopf bifurcation theorem for delayed systems is similar to the case for systems without delay (Hale & Lunel, 1993). In order for a system to be at a Hopf bifurcation, we require (1) $a = 0$, (2) $b_k \neq 0$, and (3) $\frac{da}{dD_k}|_{a=0} \neq 0$. Condition 1 is satisfied by the assumption, and condition 2 follows by substituting $|D_k| > 1$ into equation C.9. To examine condition 3, we differentiate equations C.5 and C.6, rearrange terms, and set $a = 0$, to obtain

$$\left.\frac{da}{dD_k}\right|_{a=0} = \frac{\cos\tau_d b_k + \tau D_k}{2D_k\tau_d\cos\tau_d b_k + \tau_d^2 D_k^2 + 1}. \tag{C.11}$$

Let us suppose the converse of condition 3, that is, $\frac{da}{dD_k}|_{a=0} = 0$. Then equation C.11 results in

$$\cos \tau_d b_k + \tau_d D_k = 0. \tag{C.12}$$

Combining equations C.9 and C.12 yields $\tau_d = -1/D_k^2 < 0$, which is a contradiction. Therefore, $\frac{da}{dD_k}|_{a=0} \neq 0$. This argument holds true for all $k = 0, 1, 2, \ldots$.

Consequently, equation 7.2 admits a countably infinite number of Hopf bifurcations that are characterized by a sequence of D: $\{D_0, D_1, D_2, \ldots\}$. However, we are interested only in the case where h^* changes stability. Starting with D for which every λ satisfying equation C.4 has negative real parts, loss of stability occurs when two conjugate eigenvalues cross the imaginary axis as D goes through D_k for some k. We focus on $D = D_0$ where h^* actually changes stability (Giannakopoulos & Zapp, 1999). By substituting b_0 taken from equation C.9 into equation C.10, we obtain the transcendental equation to determine D_0:

$$\arccos \frac{1}{D_0} = \tau_d \sqrt{1 - D_0^2}. \tag{C.13}$$

Given τ_d, β, τ_0, and τ_r, equations C.1 and C.13 determine the set of values $\Gamma = \{J, I_0\}$ for which the system represented by equation 7.2 is at a Hopf bifurcation. The J/I_0 parameter space is partitioned into the stable regime and the unstable or oscillatory regime by Γ. Using standard root-finding methods, we solve equations C.1 and C.13 and plot the curve Γ in Figure 8A.

Center manifold reduction and normal form calculation for retarded functional differential systems are possible (Faria & Magalhães, 1995). However, such an analysis is beyond the scope of this article. Nevertheless, it has been performed for a general class of retarded functional difference equations of which equation 7.2 is an example (Giannakopoulos & Zapp, 1999). Then the coefficient of the third-order term in the normal form of the Hopf bifurcation is generally derived. This coefficient determines the criticality of the bifurcation, namely, whether the bifurcation is subcritical or supercritical. Application of this expression to equation 7.2 shows that the Hopf bifurcation is supercritical for all values of (I_0, J, τ_d) that constitute Γ, disallowing any bistability (results not shown).

Acknowledgments

We thank John Lewis, Jason Middleton, Maurice Chacron, Jan Benda, Krisztina Salisznyo, and Benjamin Lindner for helpful comments. N.M. acknowledges financial support from the Special Postdoctoral Researchers Program of RIKEN. N.M. and K.A. acknowledge financial support from

the Advanced and Innovational Research Program in Life Sciences from the Ministry of Education, Culture, Sports, Science, and Technology, the Japanese Government. B.D. and A.L. acknowledge financial support from NSERC, Canada.

References

Abeles, M. (1991). *Corticonics*. Cambridge: Cambridge University Press.

Aihara, K., & Matsumoto, G. (1982). Temporally coherent organization and instabilities in squid giant axons. *J. Theor. Biol., 95*, 697–720.

Aviel, Y., Mehring, C., Abeles, M., & Horn, D. (2003). On embedding synfire chains in a balanced network. *Neural Comput., 15*, 1321–1340.

Bal, T., Debay, D., & Destexhe, A. (2000). Cortical feedback controls the frequency and synchrony of oscillations in the visual thalamus. *J. Neurosci., 20*(19), 7478–7488.

Berman, N. J., & Maler, L. (1999). Neural architecture of the electrosensory lateral line lobe: Adaptations for coincidence detection, a sensory searchlight and frequency-dependent adaptive filtering. *J. Experimental Biology, 202*, 1243–1253.

Billock, V. A. (1997). Very short term visual memory via reverberation: A role for the cortico-thalamic excitatory circuit in temporal filling-in during blinks and saccades? *Vision Research, 37*(7), 949–953.

Bringuier, V., Chavane, F., Glaeser, L., & Frégnac, Y. (1999). Horizontal propagation of visual activity in the synaptic integration field of area 17 neurons. *Science, 283*, 695–699.

Brunel, N. (2000). Dynamics of sparsely connected networks of excitatory and inhibitory spiking neurons. *J. Comput. Neurosci., 8*, 183–208.

Brunel, N., & Hakim, V. (1999). Fast global oscillations in networks of integrate-and-fire neurons with low firing rates. *Neural Computation, 11*, 1621–1671.

Burkitt, A. N., & Clark, G. M. (2001). Synchronization of the neural response to noisy periodic synaptic input. *Neural Computation, 13*, 2639–2672.

Buzsáki, G., & Draguhn, A. (2004). Neuronal oscillations in cortical networks. *Science, 304*, 1926–1929.

Câteau, H., & Fukai, T. (2001). Fokker-Planck approach to the pulse packet propagation in synfire chain. *Neural Networks, 14*, 675–685.

Chacron, M. J., Doiron, B., Maler, L., Longtin, A., & Bastian, J. (2003). Nonclassical receptive field mediates switch in a sensory neuron's frequency tuning. *Nature, 423*, 77–81.

Chance, F. S., Abbott, L. F., & Reyes, A. D. (2002). Gain modulation from background synaptic input. *Neuron, 35*, 773–782.

Cox, T. R., & Lewis, P. A. W. (1966). *The statistical analysis of series of events*. London: Methuen.

Damasio, A. R. (1989). The brain binds entities and events by multiregional activation from convergence zones. *Neural Computation, 1*, 123–132.

Destexhe, A., & Sejnowski, T. J. (2003). Interactions between membrane conductances underlying thalamocortical slow-wave oscillations. *Physiol. Rev., 83*, 1401–1453.

Diesmann, M., Gewaltig, M.-O., & Aertsen, A. (1999). Stable propagation of synchronous spiking in cortical neural networks. *Nature, 402*, 529–533.

Doiron, B. (2004). *Electrosensory dynamics: Dendrites and delays*. Unpublished doctoral dissertation, University of Ottawa.

Doiron, B., Chacron, M. J., Maler, L., Longtin, A., & Bastian, J. (2003). Inhibitory feedback required for network oscillatory responses to communication but not prey stimuli. *Nature, 421*, 539–543.

Doiron, B., Lindner, B., Longtin, A., Maler, L., & Bastian, J. (2004). Oscillatory activity in electrosensory neurons increases with the spatial correlation of the stochastic input stimulus. *Phys. Rev. Lett., 93*(4), 048101.

Douglas, R. J., Koch, C., Mahowald, M., Martin, K. A. C., & Suarez, H. H. (1995). Recurrent excitation in neocortical circuits. *Science, 269*, 981–985.

Faria, T., & Magalhães, L. T. (1995). Normal form for retarded functional differential equations with parameters and applications to Hopf bifurcation. *J. Differential Equations, 122*, 181–200.

Fontanini, A., Spano, P., & Bower, J. M. (2003). Ketamine-Xylazine-induced slow (<1.5 Hz) oscillations in the rat piriform (olfactory) cortex are functionally correlated with respiration. *J. Neurosci., 23*(22), 7993–8001.

Gerstner, W. (2000). Population dynamics of spiking neurons: Fast transients, asynchronous states, and locking. *Neural Computation, 12*, 43–89.

Gerstner, W., Kempter, R., van Hemmen, J. L., & Wagner, H. (1996). A neuronal learning rule for sub-millisecond temporal coding. *Nature, 383*, 76–78.

Gerstner, W., & Kistler, W. M. (2002). *Spiking neuron models*. Cambridge: Cambridge University Press.

Giannakopoulos, F., & Zapp, A. (1999). Local and global Hopf bifurcation in a scalar delay differential equation. *J. Math. Anal. Appl., 237*, 425–450.

Gilbert, C. D., & Wiesel, T. N. (1983). Clustered intrinsic connections in cat visual cortex. *J. Neurosci., 3*(5), 1116–1133.

Gray, C. M., König, P., Engel, A. K., & Singer, W. (1989). Oscillatory responses in cat visual cortex exhibit inter-columnar synchronization which reflects global stimulus properties. *Nature, 338*, 334–337.

Hale, J. K., & Lunel, S. V. (1993). *Introduction to functional differential equations*. New York: Springer Verlag.

Heiligenberg, W. (1991). *Neural nets in electric fish*. Cambridge, MA: MIT Press.

Hô, N., & Destexhe, A. (2000). Synaptic background activity enhances the responsiveness of neocortical pyramidal neurons. *J. Neurophysiol., 84*, 1488–1496.

Hopfield, J. J. (1995). Pattern recognition computation using action potential timing for stimulus representation. *Nature, 376*, 33–36.

Hunter, J. D., Milton, J. G., Thomas, P. J., & Cowan, J. D. (1998). Resonance effect for neural spike time reliability. *J. Neurophysiol., 80*, 1427–1438.

Izhikevich, E. M., Desai, N. S., Walcott, E. C., & Hoppensteadt, F. C. (2003). Bursts as a unit of neural information: Selective communication via resonance. *Trends in Neurosciences, 26*(3), 161–167.

Kistler, W. M., & De Zeeuw, C. I. (2002). Dynamical working memory and timed responses: The role of reverberating loops in the olivo-cerebellar system. *Neural Computation, 14*, 2597–2626.

Klausberger, T., Magill, P. J., Márton, L. F., Roberts, J. D. B., Cobden, P. M., Buzsáki, G., & Somogyi, P. (2003). Brain-state- and cell-type-specific firing of hippocampal interneurons *in vivo*. *Nature, 421*, 844–848.

Knight, B. W. (1972). Dynamics of encoding in a population of neurons. *Journal of General Physiology, 59*, 734–766.

Knight, B. W. (2000). Dynamics of encoding in neuron populations: Some general mathematical features. *Neural Computation, 12*, 473–518.

Kuhn, A., Aertsen, A., & Rotter, S. (2004). Neuronal integration of synaptic input in the fluctuation-driven regime. *J. Neurosci., 24*(10), 2345–2356.

Laing, C. R., & Longtin, A. (2003). Dynamics of deterministic and stochastic paired excitatory-inhibitory delayed feedback. *Neural Computation, 15*, 2779–2822.

Lindner, B., & Schimansky-Geier, L. (2002). Maximizing spike train coherence or incoherence in the leaky integrate-and-fire model. *Phys. Rev. E, 66*, 031916.

Litvak, V., Sompolinsky, H., Segev, I., & Abeles, M. (2003). On the transmission of rate code in long feedforward networks with excitatory-inhibitory balance. *J. Neurosci., 23*(7), 3006–3015.

Llinás, R. R., Grace, A. A., & Yarom, Y. (1991). *In vitro* neurons in mammalian cortical layer 4 exhibit intrinsic oscillatory activity in 10- to 50-Hz frequency range. *Proc. Natl. Acad. Sci. USA, 88*, 897–901.

Longtin, A. (1991). Noise-induced transitions at a Hopf bifurcation in a first order delay-differential equation. *Phys. Rev. A., 44*(8), 4801–4813.

Longtin, A. (1995). Mechanisms of stochastic phase locking. *Chaos, 5*(1), 209–215.

Longtin, A. (2000). Effect of noise on the tuning properties of excitable systems. *Chaos, Solitons and Fractals, 11*, 1835–1848.

Longtin, A., & St-Hilaire, M. (2000). Encoding carrier amplitude modulations via stochastic phase synchronization. *Int. J. Bifu. Chaos, 10*(10), 2447–2463.

Maex, R., & De Schutter, E. (2003). Resonant synchronization in heterogeneous networks of inhibitory neurons. *J. Neurosci., 23*(33), 10503–10514.

Marcus, C. M., & Westervelt, R. M. (1989). Stability of analog neural networks with delay. *Phys. Rev. A, 39*(1), 347–359.

Masuda, N., & Aihara, K. (2002a). Spatio-temporal spike encoding of a continuous external signal. *Neural Computation, 14*, 1599–1628.

Masuda, N., & Aihara, K. (2002b). Bridging rate coding and temporal spike coding by effect of noise. *Phys. Rev. Lett., 88*(24), 248101.

Masuda, N., & Aihara, K. (2003a). Duality of rate coding and temporal spike coding in multilayered feedforward networks. *Neural Computation, 15*, 103–125.

Masuda, N., & Aihara, K. (2003b). Ergodicity of spike trains: When does trial averaging make sense? *Neural Computation, 15*, 1341–1372.

Masuda, N., & Aihara, K. (2003c). Filtered interspike interval encoding by class II neurons. *Physics Letters A, 311*(6), 485–490.

Mehring, C., Hehl, U., Kubo, M., Diesmann, M., & Aertsen, A. (2003). Activity dynamics and propagation of synchronous spiking in locally connected random networks. *Biol. Cybern., 88*, 395–408.

Murphy, P. C., Duckett, S. G., & Sillito, A. M. (1999). Feedback connections to the lateral geniculate nucleus and cortical response properties. *Science, 286*, 1552–1554.

Nirenberg, S., & Latham, P. E. (2003). Decoding neuronal spike trains: How important are correlations? *Proc. Nat. Acad. Sci. USA, 100*(12), 7348–7353.

Plenz, D., & Kitai, S. T. (1999). A basal ganglia pacemaker formed by the subthalamic nucleus and external globus pallidus. *Nature, 400*, 677–682.

Reyes, A. D. (2003). Synchrony-dependent propagation of firing rate in iteratively constructed networks *in vitro*. *Nature Neurosci., 6*(6), 593–599.

Rinzel, J., & Ermentrout, B. (1998). Analysis of neural excitability and oscillations. In C. Koch & I. Segev (Eds.), *Methods in neuronal modeling: From ions to networks* (2nd ed., pp. 251–291). Cambridge, MA: MIT Press.

Risken, H. (1984). *The Fokker-Planck equation*. New York: Springer-Verlag.

Ritz, R., & Sejnowski, T. J. (1997). Synchronous oscillatory activity in sensory systems: New vistas on mechanisms. *Curr. Opinion in Neurobiol., 7*, 536–546.

Shadlen, M. N., & Newsome, W. T. (1998). The variable discharge of cortical neurons: Implications for connectivity, computation, and information coding. *J. Neurosci., 18*(10), 3870–3896.

Sillito, A. M., Jones, H. E., Gerstein, G. L., & West, D. C. (1994). Feature-linked synchronization of thalamic relay cell firing induced by feedback from the visual cortex. *Nature, 369*, 479–482.

Stopfer, M., Bhagavan, S., Smith, B. H., & Laurent, G. (1997). Impaired odour discrimination on desynchronization of odour-encoding neural assemblies. *Nature, 390*, 70–74.

van Rossum, M. C., W., Turrigiano, G. G., & Nelson, S. B. (2002). Fast propagation of firing rates through layered networks of noisy neurons. *J. Neurosci., 22*(5), 1956–1966.

Wilson, H. R. (1999). *Spike decisions and actions*. New York: Oxford University Press.

Received April 7, 2004; accepted March 4, 2005.